pISSN 1229-3008 eISSN 2287-6251
Progress in Superconductivity and Cryogenics
Vol.21, No.3, (2019), pp.6~12 https://doi.org/10.9714/psac.2019.21.3.006

Low-energy interband transition effects on extended Drude model analysis of optical data of correlated electron system

Jungseek Hwang*

Department of Physics, Sungkyunkwan University, Suwon, Gyeonggi-do, 61419, Republic of Korea

(Received 13 August 2019; revised or reviewed 18 September 2019; accepted 19 September 2019)

Abstract

Extended Drude model has been used to obtain information of correlations from measured optical spectra of strongly correlated electron systems. The optical self-energy can be defined by the extended Drude model formalism. One can extract the optical self-energy and the electron-boson spectral density function from measured reflectance spectra using a well-developed usual process, which is consistent with several steps including the extended Drude model and generalized Allen's formulas. Here we used a reverse process of the usual process to investigate the extended Drude analysis when an additional low-energy interband transition is included. We considered two typical electron-boson spectral density model functions for two different (normal and *d*-wave superconducting) material states. Our results show that the low-energy interband transition might give significant effects on the electron-boson spectral density function obtained using the usual process. However, we expect that the low-energy interband transition can be removed from measured spectra in a proper way if the transition is well-defined or well-known.

Keywords: extended Drude model, optical self-energy, electron-boson spectral density function, low-energy interband transition

1. INTRODUCTION

So-called strange metallicity, pseudogap, and *d*-wave superconductivity have been observed in strongly correlated copper oxide systems. One can describe electrons in these systems using an extended Drude model formalism [1-4]. An important complex optical quantity, which is called the optical self-energy [4], can be defined by the extended Drude model formalism. The correlation information between electrons can be encoded in the optical self-energy like in the quasiparticle self-energy. These two self-energies are closely related to other [5, 6]. However, the optical self-energy is more complicated quantity than the quasiparticle self-energy and is called a two-particle self-energy because both filled and empty electronic states are involved in the optical (absorption) process. The extended Drude model has been applied to many correlated electron systems and provided a lot of important and intriguing results [3, 4 ,7-12].

A measured reflectance spectrum of a strongly correlated electron system is a complicated quantity in theoretical point of view. Usually, one can obtain theoretically more easily accessible quantities like the optical conductivity, the dielectric function, from the measured reflectance spectrum in a wide spectral range using a Kramers-Kronig relation between the amplitude and phase of the complex reflection coefficient. These optical quantities will carry the information on correlation between electrons. To extract the correlation information, one can use the extended Drude model analysis. As we mentioned in the previous paragraph, the optical self-energy can be obtained from the measured spectrum using the extended Drude formalism. One can extract information on correlation like the mass enhancement factor and the inelastic scattering rate from the optical self-energy. Furthermore, one can obtain the electron-boson spectral density function, which is a more fundamental quantity than the optical self-energy, using the generalized Allen formulas [13-16]. The electron-boson spectral density function is an important quantity, which shows interactions between electrons by exchanging force-mediating bosons. From the electron-boson spectral density function one can obtain the coupling strength between electrons and estimate the superconducting transition temperature using a McMillan formula [17-19]. Through the process described above one can obtain the electron-boson spectral density function from the measured reflectance spectrum. This process consists of a series of steps (Kramers-Kronig relation, extended Drude model, and generalized Allen's formulas) and is called as a normal process [20-24]. Through an opposite order of the normal process, starting from a given electron-boson spectral density function one can get the optical conductivity and other optical constants including the reflectance. This process is called as a reverse process [25].

In this paper we used this reverse process to study low-energy interband transition effects on the extended Drude model analysis. This work was motivated by a previous study [26]. Here we clearly show low-energy interband transition effects on the electron-boson spectral density function using the reverse process. We used the same two model electron-boson spectral density functions (MMP and MMP+GP), which were used in a previously published paper [27], to avoid repeating similar calculations and for easy comparisons to the previously reported quantities. We

* Corresponding author: jungseek@skku.edu

considered normal and *d*-wave superconducting states. We observed that the interband transition (or Lorentz mode) appears as a dip in the real part of the optical self-energy and a peak-dip feature in the imaginary part. Therefore, in some way one can subtract the interband transition from the resulting total spectrum. We also observed that the resulting electron-boson spectral density functions obtained from the model systems including the low-energy interband transition using the usual process are significantly influenced by the additional interband transition near the frequency region where the transition is located.

2. THEORETICAL FORMALISM

Here we introduce the reverse process [25] in some detail for two (normal and d-wave superconducting) material states in the phase diagram of cuprates. Even though a similar description of theoretical formalism has been reported elsewhere [27] we describe it again here to help the readers. The electron-boson spectral density function is denoted by $I^2B(\omega)$, where I is the coupling constant between the mediating boson and an electron and $B(\omega)$ is the boson spectral density. We note that we use the same notations as in a published paper [27]. We calculate the imaginary part of the complex optical self-energy [$\tilde{\Sigma}^{op}(\omega) \equiv \Sigma_1^{op}(\omega) + i\Sigma_2^{op}(\omega)$] with a given model $I^2B(\omega)$ using the generalized Allen's formalisms [13] as follows:

$$-2\Sigma_2^{op}(\omega,T) \equiv \frac{1}{\tau^{op}(\omega,T)} = \int_0^\infty d\Omega\ I^2B(\Omega,\mathrm{T})K(\omega,\Omega,T) + \frac{1}{\tau_{imp}^{op}(\omega,T)}, \quad (1)$$

where $1/\tau^{op}(\omega,T)$ is the optical scattering rate, $K(\omega,\Omega,T)$ is the kernel of the generalized Allen's integral equation and $1/\tau_{imp}^{op}(\omega,T)$ is the optical impurity scattering rate. The kernels for the normal and *d*-wave superconducting states [13, 15, 28] can be expressed as

$$K(\omega,\Omega,T) = \frac{\pi}{\omega}\left[2\omega\coth\left(\frac{\Omega}{2T}\right) - (\omega-\Omega)\coth\left(\frac{\omega+\Omega}{2T}\right) + (\omega+\Omega)\coth\left(\frac{\omega-\Omega}{2T}\right)\right] \text{ (normal state) or}$$

$$K(\omega,\Omega,T) = \frac{2\pi}{\omega}(\omega-\Omega)\times \langle\Theta(\omega-2\Delta(\theta,T)-\Omega)E\left(\sqrt{1-\left[\frac{2\Delta(\theta,T)}{\omega-\Omega}\right]^2}\right)\rangle_\theta \quad (d\text{-wave SC state}), \quad (2)$$

where $\Theta(\omega)$ is the Heaviside step function, $E(\omega)$ is the complete elliptic integral of the second kind, and $<\ldots>_\theta$ represents the angular average over $\theta \in [0,\ \pi/4]$. $\Delta(\theta,T)$ is the *d*-wave superconducting gap, i.e. $\Delta(\theta,T) = \Delta(T)\cos(2\theta)$, where $\Delta(T)$ is the superconducting energy gap with the maximum gap Δ_0 at $T = 0$.

We will discuss for $T = 0$ case for simplicity. At $T = 0$, the kernels can be expressed as

$$K(\omega,\Omega) = \frac{2\pi}{\omega}\Theta(\omega-\Omega)\ (\omega-\Omega) \text{ (normal state) or}$$

$$K(\omega,\Omega,T) = \frac{2\pi}{\omega}(\omega-\Omega)\,\langle\Theta(\omega-2\Delta(\theta)-\Omega)E\left(\sqrt{1-\left[\frac{2\Delta(\theta)}{\omega-\Omega}\right]^2}\right)\rangle_\theta \quad (d\text{-wave SC state}), \quad (3)$$

where $\Delta(\theta) = \Delta_0\cos(2\theta)$.

The impurity optical scattering rate at $T = 0$ can be expressed as

$$\frac{1}{\tau_{imp}^{op}(\omega)} = \frac{1}{\tau_{imp}} \text{ (for normal state) or}$$

$$\frac{1}{\tau_{imp}^{op}(\omega)} = \frac{1}{\tau_{imp}}\,\langle E\left(\sqrt{1-\left[\frac{2\Delta(\theta)}{\omega}\right]^2}\right)\rangle_\theta, \ (d\text{-wave SC state}) \quad (4)$$

where $1/\tau_{imp}$ is the constant impurity scattering rate. The impurity scattering rate in the SC state shows a strong frequency-dependence near twice of the *d*-wave superconducting gap.

We obtain the real part of the optical self-energy from the obtained imaginary part using the Kramers-Kronig relation between them as

$$-2\Sigma_1^{op}(\omega) \equiv \left[\frac{m_{op}^*(\omega)}{m_b} - 1\right]\omega = \frac{2\omega}{\pi}P\int_0^\infty d\omega'\frac{[-2\Sigma_2^{op}(\omega)]}{\omega'^2-\omega^2}, \quad (5)$$

where $m_{op}^*(\omega)$ is the optical effective mass, m_b is the band mass, and P represents the principle part of the improper integral. The mass enhancement function $[m_{op}^*(\omega)/m_b]$ can be expressed in terms of the optical coupling function $[\lambda^{op}(\omega)]$ as $m_{op}^*(\omega)/m_b = \lambda^{op}(\omega) + 1$.

In the extended Drude model formalism [2, 4] we calculate the complex optical conductivity [$\tilde{\sigma}(\omega) \equiv \sigma_1(\omega) + i\sigma_2(\omega)$] as

$$\tilde{\sigma}(\omega) = \frac{i}{4\pi}\frac{\Omega_p^2}{\omega+[-2\tilde{\Sigma}^{op}(\omega)]}, \quad (6)$$

where Ω_p is the plasma frequency, which is contributed from itinerant correlated electrons. Using the relationships between optical quantities we can calculate other optical constants including reflectance spectrum from the complex optical conductivity [29]. The complex optical dielectric function $[\tilde{\epsilon}(\omega) \equiv \epsilon_1(\omega) + i\epsilon_2(\omega)]$ has a relationship with the optical conductivity as, $\tilde{\epsilon}(\omega) = \epsilon_H + i\frac{4\pi}{\omega}\tilde{\sigma}(\omega)$, where ϵ_H is the background high frequency dielectric constant. Using a well-known Fresnel's equation, the normal incident reflectance $[R(\omega)]$ can be obtained as, $R(\omega) = |[\sqrt{\tilde{\epsilon}(\omega)}-1]/[\sqrt{\tilde{\epsilon}(\omega)}+1]|^2$.

3. RESULTS OF MODEL CALCULATIONS AND DISCUSSIONS

For theoretical calculations we considered two (normal and *d*-wave superconducting (SC)) states with two typical input $I^2B(\omega)$ models [23, 27, 30]. We note that these results also have been reported in a published literature [27]. The two typical $I^2B(\omega)$ are modelled for antiferromagnetic spin-fluctuations (AF-SF) at high and low temperatures, respectively. The AF-SF at high-T consists of the broad Millis, Monien, and Pines (MMP) mode [31] alone and the other AF-SF at low-T consists of two components: one sharp Gaussian peak (GP) and the broad MMP mode [31]. The temperature-dependent and doping-dependent evolutions of $I^2B(\omega)$ are well-established by various spectroscopy techniques including optical spectroscopy [4, 23, 24, 30, 32-36]. In the low-left corner of Fig. 1 we show the two typical (MMP and MMP+GP) model $I^2B(\omega)$. The MMP+GP model can be expressed in a mathematical form as $I^2B(\omega) = \frac{A_{MMP}\omega}{\omega^2+\omega_{SF}^2} + A_{GP}/\left[\sqrt{2\pi\left(\frac{W}{2.35}\right)^2}\right]\exp\{-(\omega-\Omega_R)^2/[2(W/2.35)^2]\}$, where A_{MMP} (= 50 meV) and ω_{SF} (= 60 meV) are, respectively, the amplitude and the characteristic frequency of the MMP mode and A_{GP} (= 50 meV), W (= 10 meV), and Ω_R (= 30 meV) are, respectively, the amplitude, width, and center frequency of the sharp GP mode. The MMP model can be expressed as $I^2B(\omega) = \frac{A_{MMP}\omega}{\omega^2+\omega_{SF}^2}$ with the same parameters as in the MMP mode above. The correlation constant (λ) can be defined in terms of $I^2B(\omega)$ as $\lambda \equiv 2\int_0^{\omega_{cutoff}} d\Omega\, I^2B(\Omega)/\Omega$, where ω_{cutoff} is the cutoff frequency, which is 600 meV for our case. The calculated correlation constants of the MMP and MMP+GP models are 2.42 and 5.83, respectively.

In Fig. 1(a) and 1(b) the calculated imaginary parts of the optical self-energy of the two (normal and *d*-wave SC) states with the two typical input $I^2B(\omega)$ (MMP and MMP+GP models) for, respectively, $1/\tau_{imp}$= 0.0 meV and 30.0 meV. For the *d*-wave SC state, below and just above $2\Delta_0$ of 60 meV we observe impurity effects as we expect from Eq. (4). Each calculated imaginary part of the optical self-energy for $1/\tau_{imp}$= 30 meV in high frequency region is higher than the corresponding self-energy with $1/\tau_{imp}$= 0.0 meV by roughly 30 meV. For the normal state the imaginary part of the optical self-energy is vertically shifted by exactly 30 meV in the whole spectral range compared with the corresponding self-energy with $1/\tau_{imp}$= 0.0 meV. All imaginary parts of the self-energies for the same model $I^2B(\omega)$ are getting merged at high-frequency region. In principle, the imaginary part of the optical self-energy for $1/\tau_{imp}$= 0.0 meV will be saturated to $2\pi\times$ (the area under $I^2B(\omega)$) [37]. The expected saturation values for the MMP and MMP+GP models are 724 meV and 1038 meV, respectively. The imaginary parts of the optical self-energy of normal and *d*-wave SC states for the MMP+GP model show a strong scattering rate jump near the center frequency of the sharp GP peak. From this jump one can estimate the strength of the GP mode. The onset frequency of the jump depends upon the (normal and *d*-wave SC) states of materials; the onset frequencies for the normal and *d*-wave SC states are roughly Ω_R and $\Omega_R + 2\Delta_0$, respectively.

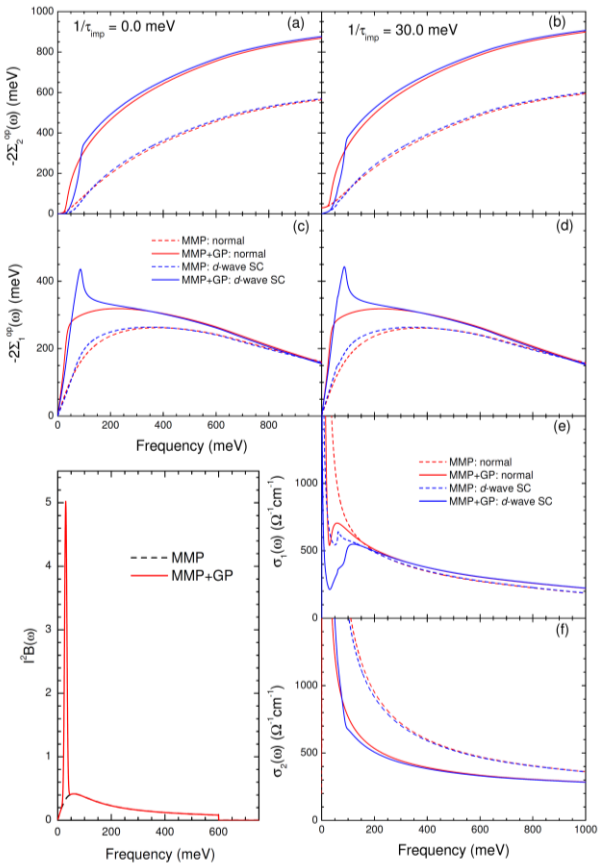

Fig. 1. (Color online) Two typical input model electron-boson spectral density functions, $I^2B(\omega)$: the MMP and MMP+GP models are shown in the low-left corner. (a) and (b) The calculated imaginary parts of the optical self-energy of the two (normal and *d*-wave SC) states for $1/\tau_{imp}$ = 0.0 and 30.0 meV respectively. (c) and (d) The corresponding real parts of the optical self-energy of the two (normal and *d*-wave SC) for $1/\tau_{imp}$= 0.0 and 30.0 meV, respectively. (e) and (f), respectively, the real and imaginary parts of the calculated optical conductivity of the two (normal and *d*-wave SC) states for $1/\tau_{imp}$= 30.0 meV.

In Fig. 1(c) and 1(d) we show the corresponding real parts of the optical self-energy, which are obtained from the imaginary parts in a wide spectral range from 0 to 7000 meV using the Kramers-Kronig relation, Eq. (5). The real part of the optical self-energy carries information on the resonance interaction energy between electrons by exchanging the mediating bosons at each frequency. The width of the resonance energy is determined by the imaginary part of the optical self-energy. This real part of the optical self-energy can also carry the information of the effective mass of charge carriers caused by the interaction. For the normal state, the real part of the optical self-energy is independent of the impurity scattering rate since the impurity scattering rate is a constant. For the broad MMP model case, the different (normal and *d*-wave SC) material

states are not very resolvable since all self-energies are quite similar to each other. In contrast, for the MMP+GP model case, the different (normal and *d*-wave SC) material states are well-resolvable since the sharp GP mode shows different shapes for the different material states. Therefore, one may be able to study the doping- and temperature-dependent evolutions of the GP mode in the phase diagram of the cuprates as reported by previous studies [4, 23, 24, 27] by monitoring the intensity, position, and/or width of the GP mode [27].

In Fig. 1(e) and 1(f) we show, respectively, the real and imaginary parts of the optical conductivity obtained from the optical self-energy for $1/\tau_{imp}$ = 30.0 meV using the extended Drude model formalism, Eq. (6). Here we used the plasma frequency (Ω_p) of 2000 meV. In the normal state, the real parts of the optical conductivity of the MMP+GP shows a sharp dip near the center frequency of the GP mode. The dip roughly divides the spectral weight of itinerant electrons into two (coherent and incoherent) components. In the *d*-wave SC state, the real parts of the optical conductivity of the MMP and MMP+GP models show clear features near $2\Delta_0$ energy due to the impurity scattering rate. The MMP+GP model shows an addition feature near $\Omega_R + 2\Delta_0$ energy. Furthermore, descriptions about the complex optical conductivity spectra for all phases including the pseudogap phase can be found in a published literature [27].

4. LOW-ENERGY INTERBAND TRANSITION EFFECTS ON EXTENDED DRUDE MODEL ANALYSIS

There are several important issues on optical spectrum analysis using the extended Drude model [26, 38-41]. In this section we revisited the issue on low-energy interband transition effect on the extended Drude model analysis, which was previously discussed by Benfatto *et al.* [26], since we would like to focus on low-energy interband transition effect on the electron-boson spectral density function, $I^2B(\omega)$.

We investigate effects of a low-energy interband transition to the complex optical self-energy, which has been raised by a recent theoretical report on iron-based superconductivity [26]. The interband transition can be modelled with a Lorentz mode. For this investigation, we considered three different cases. In each case we included a Lorentz mode in the existing model system. We considered three different Lorentz modes with different center frequencies (Ω_{L0}) of 100, 300, and 500 meV, the same width (Γ_L) of 100 meV, and the same plasma frequency (Ω_{Lp}) of 400 meV. We added the Lorentz mode to the complex optical conductivity [$\tilde{\sigma}(\omega)$] previously calculated through the reverse process as

$$\tilde{\sigma}^{total}(\omega) = \tilde{\sigma}(\omega) + \frac{i}{4\pi}\frac{[-\Omega_{Lp}^2]}{\Omega_{L0}^2-\omega^2-i\Gamma_L\omega}, \qquad (7)$$

where $\tilde{\sigma}^{total}(\omega)$ is the total complex optical conductivity. We note that, since in this situation we have both intraband and interband transitions in this model system, strictly speaking, we cannot apply the extended Drude model analysis to this system. However, here we assumed that the system did not have the interband transition and applied the extended Drude model analysis to the model system. We obtained the total complex optical self-energy ($-2\tilde{\Sigma}^{op,total}(\omega) \equiv -2\Sigma_1^{op,total}(\omega) + i[-2\Sigma_2^{op,total}(\omega)]$) from the total optical conductivity of the model system using the extended Drude model as

$$-2\tilde{\Sigma}^{op,total}(\omega) = \mathrm{i}\frac{[\Omega_p^{total}]^2}{4\pi}\frac{1}{\tilde{\sigma}^{total}(\omega)} - \omega, \qquad (8)$$

where Ω_p^{total} is the total plasma frequency, i.e., $\Omega_p^{total} \equiv \sqrt{\Omega_p^2 + \Omega_{Lp}^2}$, which Ω_p is the plasma frequency used previously, i.e., 2000 meV. In Fig. 2 (with Ω_{L0} = 100 meV), Fig. 3 (with Ω_{L0} = 300 meV) and Fig. 4 (with Ω_{L0} = 500 meV) we show the total optical conductivity [(a)-(d) frames] and total optical self-energy [(e)-(h) frames] along with the corresponding previously calculated ones [i.e., $\tilde{\sigma}(\omega)$ and $-2\tilde{\Sigma}^{op}(\omega)$] of the normal and *d*-wave SC states with $1/\tau_{imp}$ = 30.0 meV for the MMP and MMP+GP models. The total optical self-energies for all the three different interband transition cases show basically the same characteristic features associated with the additional Lorentz mode; the Lorentz mode appears as a dip in the real part of the total self-energy and a peak-dip feature in the imaginary part.

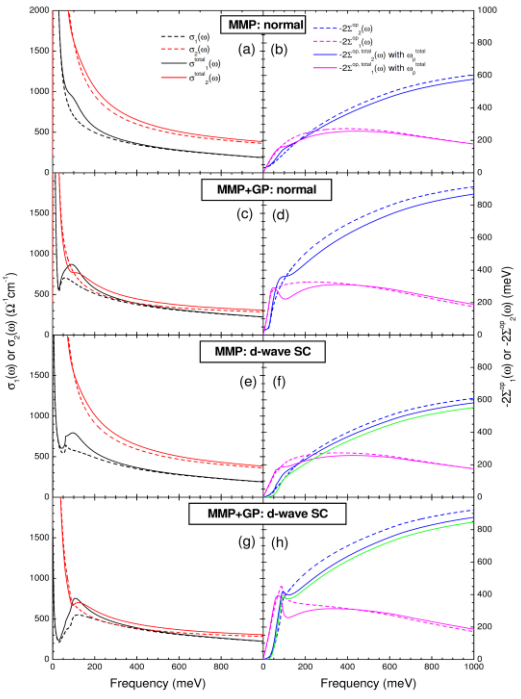

Fig. 2. (Color online) The complex optical conductivities [(a)-(d)] and the corresponding complex optical self-energies [(e)-(h)] of the MMP and MMP+GP models for the normal and *d*-wave SC phases and $1/\tau_{imp}$ = 30.0 meV cases. We also show the resulting corresponding quantities for the cases including the low-energy interband transition with the center frequency (Ω_{L0}) of 100 meV, the width (Γ_L) of 100 meV, and the plasma frequency (Ω_{Lp}) of 400 meV.

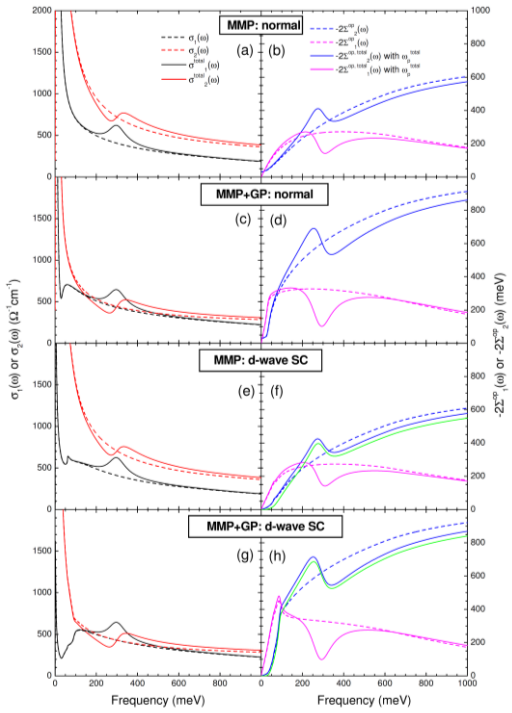

Fig. 3. (Color online) The complex optical conductivities [(a)-(d)] and the corresponding complex optical self-energies [(e)-(h)] of the MMP and MMP+GP models for the normal and *d*-wave SC phases and $\mathbf{1/\tau_{imp}}$ = 30.0 meV cases. We also show the resulting corresponding quantities for the cases including the low-energy interband transition with the center frequency ($\boldsymbol{\Omega_{L0}}$) of 300 meV, the width ($\boldsymbol{\Gamma_L}$) of 100 meV, and the plasma frequency ($\boldsymbol{\Omega_{Lp}}$) of 400 meV.

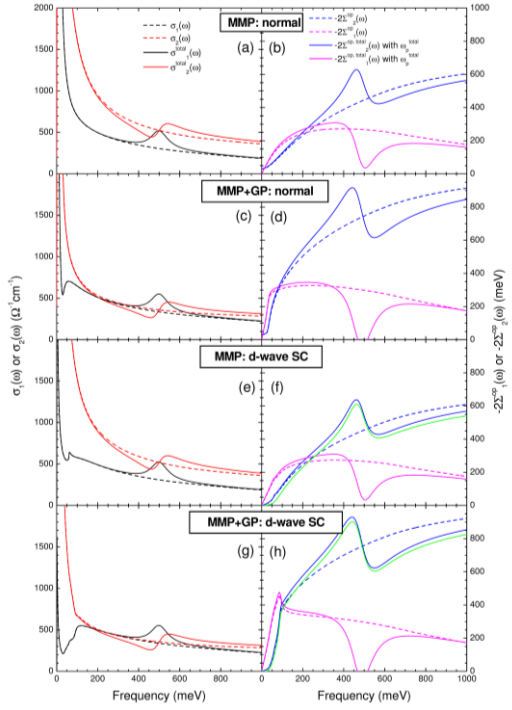

Fig. 4. (Color online) The complex optical conductivities [(a)-(d)] and the corresponding complex optical self-energies [(e)-(h)] of the MMP and MMP+GP models for the normal and *d*-wave SC phases and $\mathbf{1/\tau_{imp}}$ = 30.0 meV cases. We also show the resulting corresponding quantities for the cases including the low-energy interband transition with the center frequency ($\boldsymbol{\Omega_{L0}}$) of 500 meV, the width ($\boldsymbol{\Gamma_L}$) of 100 meV, and the plasma frequency ($\boldsymbol{\Omega_{Lp}}$) of 400 meV.

Interestingly, the peak-dip feature in the imaginary part seems to be quite similar to that in the imaginary part of the optical self-energy in a published literature [42], where the optical self-energy was obtained for a case of a complete suppression in the density of states with similar MMP and MMP+GP models. The complete suppression (or a gap) in the density of states may cause a low-energy interband transition. Here we demonstrated how the additional Lorentz mode appears in the real and imaginary parts of optical self-energy; this may be useful information to check whether the low-energy interband transition exists in measured spectra and to provide a hint how one can get rid of the low-energy interband transition from measured spectra. However, if the low-energy interband transition is not very well-defined (or sharp and/or strong enough) the expected (dip or dip-peak) features will not be pronounced. We note that if the low-energy interband transition is well-known it can be removed from measured optical conductivity spectra beforehand application of the extended Drude model analysis as shown in a recent published literature [43].

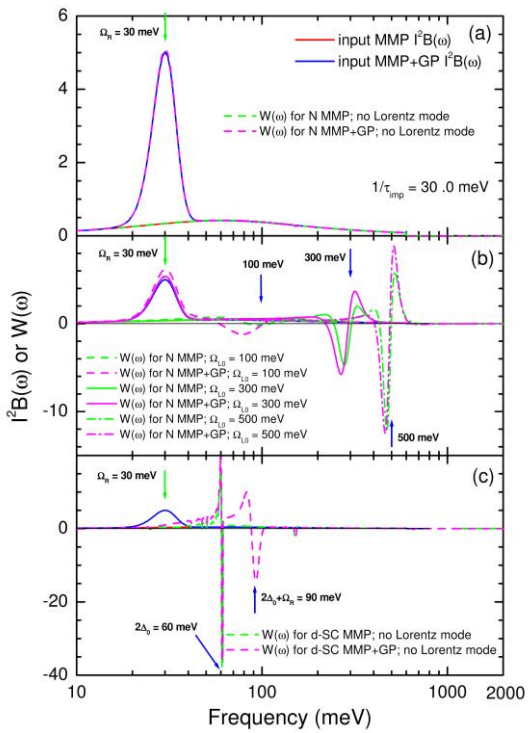

Fig. 5. (Color online) The extracted electron-boson spectral density function, $W(\omega)$, using the 2nd derivative method along with the input MMP and MMP+GP $I^2B(\omega)$ models. (a) $W(\omega)$ obtained from the imaginary part of the optical self-energy of the normal state for the MMP and MMP+GP models without including the additional Lorentz mode along with the input MMP and MMP+GP $I^2B(\omega)$ models. (b) $W(\omega)$ obtained from the imaginary part of the optical self-energy of the normal state for the MMP and MMP+GP models including the additional Lorentz mode along with the input MMP and MMP+GP $I^2B(\omega)$ models. We note

that we considered the three different Lorentz modes with the same shape but located at different frequencies. (c) $W(\omega)$ obtained from the imaginary parts of the optical self-energy of the *d*-wave SC state for the MMP and MMP+GP models without including the additional Lorentz mode along with the input MMP and MMP+GP $I^2B(\omega)$ models.

We extracted the electron-boson spectral density function using a formula, which is an exact one only for normal state at $T = 0$, $I^2B(\omega) = \left(\frac{1}{2\pi}\right) d^2\{\omega[-2\Sigma_2^{op}(\omega)]\}/d^2\omega$ [44]; this formula can be directly derived from the normal case of Eq. (3). Sometimes the resulting $I^2B(\omega)$ is denoted as $W(\omega)$ and this approach is known as the 2nd derivative method. Researchers have used this method for obtaining approximate $I^2B(\omega)$ from measured optical spectra in normal state at low temperatures and even in superconducting state [28, 45]. In Fig. 5 we show the extracted $W(\omega)$ for several cases [(a) normal state without including the interband transition, (b) normal state with the three different interband transitions, and (c) *d*-wave SC state without including the interband transition) using the 2nd derivative method and compare them with the input $I^2B(\omega)$ of MMP and MMP+GP models. In Fig. 5(a) we show $W(\omega)$ extracted from the imaginary parts of the optical self-energy of normal state for the MMP and MMP+GP models along with the input $I^2B(\omega)$. As we expected, the extracted $W(\omega)$ are the same as the corresponding input $I^2B(\omega)$. In Fig. 5(b) we show $W(\omega)$ extracted from the imaginary parts of the total optical self-energy of MMP and MMP+GP models in normal state separately including the three low-energy interband transitions with different center frequencies (Ω_{L0} = 100, 300, and 500 meV). For the case including the Lorentz mode with Ω_{L0} = 100 meV we observe artificial features [strong deviations from the input$I^2B(\omega)$] in the $W(\omega)$ of both MMP and MMP+GP models near 100 meV; a section of the artificial feature is negative. As the position of the Lorentz mode moves to higher energy the artificial feature also moves to higher energy and its intensity is getting stronger (or is better-defined). When the Lorentz mode is located at 500 meV in the energy region below 200 meV the $W(\omega)$ of both MMP and MMP+GP models agree with the corresponding input $I^2B(\omega)$. In Fig. 5(c) we show $W(\omega)$ obtained from the imaginary parts of the optical self-energy of MMP and MMP+GP models without including the Lorentz mode in *d*-wave SC state using the 2nd derivative method. As we previously mentioned, strictly speaking, the 2nd derivative method is applicable to only the imaginary parts of the optical self-energy *in normal state* at low temperatures. The resulting $W(\omega)$ of both MMP and MMP+GP in *d*-wave SC state show significant disagreements compared with the corresponding input $I^2B(\omega)$; $W(\omega)$ of both MMP and MMP+GP model show very sharp peak-dip features (or singularities) at $2\Delta_0$ (60 meV). $W(\omega)$ of the MMP+GP model shows an additional strong peak-dip structure near $2\Delta_0 + \Omega_R$ (90 meV). A similar study but with a different approach has been done for copper oxide superconducting (cuprate) systems [46] and the authors found some interesting singularities in the optical response of cuprate systems.

5. CONCLUSIONS

The complex optical self-energies of two different (normal and *d*-wave SC) states for the two typical MMP and MMP+GP models, $I^2B(\omega)$, were obtained using the generalized Allen's formulas and the Kramers-Kronig relation between the real and imaginary parts of the optical self-energy. The corresponding complex optical conductivities were obtained from the complex optical self-energy using the extended Drude model formalism. We investigated the additional low-energy interband transition effects on the extended Drude model formalism and found that the additional interband transition can give significant effects on the resulting $I^2B(\omega)$. However, the interband transition might appropriately be removed from the total spectrum if it is well-known or well-defined. We hope that this paper helps researchers to obtain the interaction information from measured optical spectra of strongly correlated electron systems with low-energy interband transitions, like Fe-based superconductors, using extended Drude model.

ACKNOWLEDGMENT

We acknowledge the financial support from the National Research Foundation of Korea (NRFK Grant No. 2017R1A2B4007387).

REFERENCES

[1] Hazime Mori, "A continued-fraction representation of the time-correlation functions," *Prog. Theor. Phys*., vol. 34, pp. 399, 1965.
[2] W. Gotze and P. Wolfle, "Homogeneous dynamical conductivity of simple metals," *Phys. Rev. B*, vol. 6, pp. 1226, 1972.
[3] A. V. Puchkov, D. N. Basov, and T. Timusk, "The pseudogap state in high-Tc superconductors: an infrared study," *J. Phys.: Cond. Matter*, vol. 8, pp. 10049, 1996.
[4] J. Hwang, T. Timusk, and G. D. Gu, "High-transition-temperature superconductivity in the absence of the magnetic-resonance mode," *Nature (London)*, vol. 427, pp. 714, 2004.
[5] J. P. Carbotte, E. Schachinger, and J. Hwang, "Boson structures in the relation between optical conductivity and quasiparticle dynamics," *Phys. Rev. B*, vol. 71, pp. 054506, 2005.
[6] J. Hwang, E. J. Nicol, T. Timusk, A. Knigavko, and J. P. Carbotte, "High energy scales in the optical self-energy of the cuprate superconductors," *Phys. Rev. Lett.*, vol. 98, pp. 207002, 2007.
[7] B. C. Webb, A. J. Sievers, and T. Mihalisin, "Observation of an energy- and temperature-dependent carrier mass for mixed-valence CePd3," *Phys. Rev. Lett.*, vol. 57, pp. 1951, 1986.
[8] P. E. Sulewski, A. J. Sievers, M. B. Maple, M. S. Torikachvili, J. L. Smith, and Z. Fisk, "Far-infrared absorptivity of UPt3," *Phys. Rev. B*, vol. 38, pp. 5338, 1988.
[9] G. A. Thomas, J. Orenstein, D. H. Rapkine, M. Capizzi, A. J. Millis, R. N. Bhatt, L. F. Schneemeyer, and J. V. Waszczak, "Y $Ba_2Cu_3O_{7-\delta}$ electrodynamics of crystals with high reflectivity," *Phys. Rev. Lett.*, vol. 61, pp. 1313, 1988.
[10] A. M. Awasthi, L. Degiorgi, G. Gruner, Y. Dalichaouch, and M. B. Maple, "Complete optical spectrum of $CeAl_3$," *Phys. Rev. B*, vol. 48, pp. 10692, 1993.
[11] S. V. Dordevic, D. N. Basov, N. R. Dilley, E. D. Bauer, and M. B. Maple, "Hybridization gap in heavy fermion compounds," *Phys. Rev.*

Lett., vol. 86, pp. 684, 2001.
[12] P. Tran, S. Donovan, and G. Gruner, "Charge excitation spectrum in UPt_3," *Phys. Rev. B*, vol. 65, pp. 205102, 2002.
[13] P. B. Allen, "Electron-phonon effects in the infrared properties of metals," *Phys. Rev. B*, vol. 3, pp. 305, 1971.
[14] B. Mitrovic and M. A. Fiorucci, "Effects of energy dependence in the electronic density of states on the far-infrared absorption in superconductors," *Phys. Rev. B*, vol. 31, pp. 2694, 1985.
[15] S. V. Shulga, O. V. Dolgov, and E. G. Maksimov, "Electronic states and optical spectra of HTSC with electron-phonon coupling," *Physica C*, vol. 178, pp. 266, 1991.
[16] S. G. Sharapov and J. P. Carbotte, "Effects of energy dependence in the quasiparticle density of states on far-infrared absorption in the pseudogap state," *Phys. Rev. B*, vol. 72, pp. 134506, 2005.
[17] W. L. McMillan and J. M. Rowell, "Lead phonon spectrum calculated from superconducting density of states," *Phys. Rev. Lett*., vol. 14, pp. 108, 1965.
[18] J. Hwang, E. Schachinger, J. P. Carbotte, F. Gao, D. B. Tanner, and T. Timusk, "Bosonic spectral density of epitaxial thin-film $La_{1.83}Sr_{0.17}CuO_4$ superconductors from infrared conductivity measurements," *Phys. Rev. Lett.*, vol. 100, pp. 137005, 2008.
[19] J. Hwang, "Electron-boson spectral density function of underdoped $Bi_2Sr_2CaCu_2O_{8+\delta}$ and $YBa_2Cu_3O_{6.50}$," *Phys. Rev. B*, vol. 83, pp. 014507, 2011.
[20] R. T. Collins, Z. Schlesinger, F. Holtzberg, P. Chaudhari, and C. Field, "Reflectivity and conductivity of $YBa_2Cu_3O_7$," *Phys. Rev. B*, vol. 39, pp. 6571, 1989.
[21] J. P. Carbotte, "Properties of boson-exchange superconductors," *Rev. Mod. Phys*., vol. 62, pp. 1027, 1990.
[22] E. Schachinger and J. P. Carbotte, "Coupling to spin fluctuations from conductivity scattering rates," *Phys. Rev. B*, vol. 62, pp. 9054, 2000.
[23] J. Hwang, J. Yang, T. Timusk, S. G. Sharapov, J. P. Carbotte, D. A. Bonn, R. Liang, and W. N. Hardy, "*a*-axis optical conductivity of detwinned ortho-II $YBa_2Cu_3O_{6.50}$," *Phys. Rev. B*, vol. 73, pp. 014508, 2006.
[24] J. Hwang, T. Timusk, E. Schachinger, and J. P. Carbotte, "Evolution of the bosonic spectral density of the high-temperature superconductor $Bi_2Sr_2CaCu_2O_{8+\delta}$," *Phys. Rev. B*, vol. 75, pp. 144508, 2007.
[25] Jungseek Hwang, "Reverse process of usual optical analysis of boson-exchange superconductors: impurity effects on *s*- and *d*-wave superconductors," *J. Phys.: Condens. Matter*, vol. 27, pp. 085701, 2015.
[26] L. Benfatto, E. Cappelluti, L. Ortenzi, and L. Boeri, "Extended Drude model and role of interband transitions in the midinfrared spectra of pnictides," *Phys. Rev. B*, vol. 83, pp. 224514, 2011.
[27] Jungseek Hwang, "Analysis of optical data using extended Drude model and generalized Allen's formulas," *J. Phys.: Condens. Matter*, vol. 30, pp. 405604, 2018.
[28] E. Schachinger, D. Neuber, and J. P. Carbotte, "Inversion techniques for optical conductivity data," *Phys. Rev. B*, vol. 73, pp. 184507, 2006.
[29] Frederick Wooten, *Optical Properties of Solids.* Academic, New York, 1972. (Note: Key material on page 176).
[30] J. P. Carbotte, T. Timusk, and J. Hwang, "Bosons in high-temperature superconductors: an experimental survey," *Reports on Progress in Physics*, vol. 74, pp. 066501, 2011.
[31] A. J. Millis, H. Monien, and D. Pines, "Phenomenological model of nuclear relaxation in the normal state of $YBa_2Cu_3O_7$," *Phys. Rev. B*, vol. 42, pp. 167, 1990.
[32] Pengcheng Dai, H. A. Mook, S. M. Hayden, G. Aeppli, T. G. Perring, R. D. Hunt, and F. Doguan, "The magnetic excitation spectrum and thermodynamics of high-T_c superconductors," *Science*, vol. 284, pp. 1344, 1999.
[33] H. F. Fong, P. Bourges, Y. Sidis, L. P. Regnault, J. Bossy, A. Ivanov, D. L. Milius, I. A. Aksay, and B. Keimer, "Spin susceptibility in underdoped $YBa_2Cu_3O_{6+x}$," *Phys. Rev. B*, vol. 61, pp. 14773, 2000.
[34] P. D. Johnson, T. Valla, A. V. Fedorov, Z. Yusof, B. O. Wells, Q. Li, A. R. Moodenbaugh, G. D. Gu, N. Koshizuka, C. Kendziora, Sha Jian, and D. G. Hinks, *Phys. Rev. Lett.*, vol. 87, pp. 177007, 2001.
[35] T. Valla, T. E. Kidd, W.-G. Yin, G. D. Gu, P. D. Johnson, Z.-H. Pan, and A. V. Fedorov, *Phys. Rev. Lett.*, vol. 98, pp. 167003, 2007.
[36] Wentao Zhang, Guodong Liu, Lin Zhao, Haiyun Liu, Jianqiao Meng, Xiaoli Dong, Wei Lu, J. S. Wen, Z. J. Xu, G. D. Gu, T. Sasagawa, Guiling Wang, Yong Zhu, Hongbo Zhang, Yong Zhou, Xiaoyang Wang, Zhongxian Zhao, Chuangtian Chen, Zuyan Xu, and X. J. Zhou, *Phys. Rev. Lett.*, vol. 100, pp. 107002, 2008.
[37] J. Hwang, J. Yang, J. P. Carbotte, and T. Timusk, "Manifestation of the pseudogap in ab-plane optical characteristics," *J. Phys. Condens. Matter*, vol. 20, pp. 295215, 2008.
[38] S. V. Dordevic, D. van der Marel, and C. C. Homes, "Fate of quasiparticles in the superconducting state," *Phys. Rev. B*, vol. 90, pp. 174508, 2014.
[39] Jungseek Hwang, "Intrinsic temperature-dependent evolutions in the electron-boson spectral density obtained from optical data," *Scientific Reports*, vol. 6, pp. 23647, 2016.
[40] E. Schachinger and J. P. Carbotte, "Optical properties of bogoliubov quasiparticles," *Phys. Rev. B*, vol. 95, pp. 144516, 2017.
[41] Jungseek Hwang, *arXiv cond-mat*, page 1907.13326, 2019.
[42] J. Hwang, "Simulation of a hump structure in the optical scattering rate within a generalized Allen formalism and its application to copper oxide systems," *J. Phys. Condens. Matter*, vol. 25, pp. 295701, 2013.
[43] Jungseek Hwang, "Electron–boson spectral density function of correlated multiband systems obtained from optical data: $Ba_{0.6}K_{0.4}Fe_2As_2$ and LiFeAs," *J. Phys.: Condens. Matter*, vol. 28, pp. 125702, 2016.
[44] F. Marsiglio, T. Startseva, and J. P. Carbotte, "Inversion of K3C60 reflectance data," *Phys. Lett. A*, vol. 245, pp. 172, 1998.
[45] J. P. Carbotte, E. Schachinger, and D. N. Basov, "Coupling strength of charge carriers to spin fluctuations in high-temperature superconductors," *Nature (London)*, vol. 401, pp. 354, 1999.
[46] Ar. Abanov, A. V. Chubukov, and J. Schmalian, "Singularities in the optical response of cuprates," *Phys. Rev. B*, vol. 63, pp. 180510(R), 2001.